DUAL ACCELEROMETER USAGE STRATEGY FOR ONBOARD SPACE NAVIGATION

Renato Zanetti[*] and Chris D'Souza[†]

This work introduces a dual accelerometer usage strategy for onboard space navigation. In the proposed algorithm the accelerometer is used to propagate the state when its value exceeds a threshold and it is used to estimate its errors otherwise. Numerical examples and comparison to other accelerometer usage schemes are presented to validate the proposed approach.

INTRODUCTION

In the presence of significant and consistent non-gravitational accelerations, accelerometer measurements are often used in lieu of analytical expressions to propagate the state of aerospace vehicles in model-based estimation algorithms such as the Kalman filter [1, 2]. In space applications, accelerometers are often used to propagate the state of the vehicle through a translational maneuver, or "burn". At all other times non-gravitational forces are usually much smaller than the accuracy of most commercially available accelerometers, therefore space vehicles commonly threshold the acceleromter, i.e. they use it only when the measurements are above a predetermined value [3]. Accelerometer thresholding is also referred to as accelerometer gating. The Space Shuttle rendezvous and proximity operations program (RPOP), for example, employs this strategy [4].

Rarely accelerometers are used as external measurements to update the state of the vehicle. One example of this approach is Ref. [5] in which accelerometers are used in conjunction with a filter bank for Mars entry navigation. Under this type of implementation, a model of the non-gravitational forces is required. When on a launch pad a vehicle is stationary with respect to Earth and the predicted accelerometer measurement is very easily obtained. Pre-launch operations therefore commonly employ accelerometer measurements to update the estimate of its repeatable errors, such as biases, misalignments, and scale factors.

Accelerometers usually have two types of repeatable biases. A constant bias (sometimes represented as a first order Markov process [6] with very large time constant of the order of 24 hours) and a faster changing Markov process with time constant of around one hour. Velocity random walk (VRW) also corrupts the measurement, but this source of error

---

[*]Senior Member of the Technical Staff, Vehicle Dynamics and Controls, The Charles Stark Draper Laboratory, 17629 El Camino Real, Suite 470, Houston, Texas, 77058. rzanetti@draper.com

[†]GN&C Autonomous Flight Systems Engineer, Aeroscience and Flight Mechanics Division, NASA Johnson Space Center EG6, 2101 NASA Parkway, Houston, Texas, 77058. chris.dsouza@nasa.gov

is not estimable because it is white acceleration noise. In the standard accelerometer usage by space vehicles the accelerometer errors are estimated from external measurements through their correlation to other states. This correlation is built during maneuvers at which times the accelerometer measurement is incorporated into the filter dynamics. In between maneuvers the accelerometer measurement is not used at all, therefore the estimate of the one-hour Markov bias degrades, which results in a worst navigation performance during the next maneuver. For vehicles with small thrusters and maneuvers far apart, this approach is often not sufficient to meet mission goals. A common practice for these vehicles is to use a simple averaging scheme to estimate the accelerometer bias prior to maneuvers. This average is carried outside the navigation filter, therefore no correlation between the filter error and the accelerometer bias estimation error is taken into account when formulating a navigation solution.

This work introduces a dual accelerometer usage strategy for onboard space navigation. In the proposed algorithm the accelerometer is used to propagate the state when its value exceeds a threshold and it is used to estimate its errors otherwise. The paper is organized as follows: accelerometer thresholding is first introduced, the navigation algorithm is then presented and validated with numerical simulation, finally conclusions are drawn.

ACCELEROMETER THRESHOLDING

This section presents a simple example to show the need of accelerometer thresholding in spacecraft navigation. Outside of thrust, drag is usually the biggest non-gravitational acceleration source in low Earth orbit (LEO). The international space station (ISS) is used as an example to quantify the contribution of drag. The ISS is a large structure placed at an altitude of 400 km and is subject to high drag. A 2008 analysis from the European Space Agency[*] finds that the ISS coefficient of drag is 2.07, the frontal area between 700 and 2300m^2 depending on the configuration, and the yearly average air density 3.98 10^{-12}kg/m^3. Assuming a configuration with frontal area 1000m^2 the drag acting on the ISS is 0.25N. The mass of ISS was 2.5 10^5kg in 2008, resulting in a drag acceleration of 10^{-6}m/s^2 or 0.1μg.

A relatively good accelerometer can have a one hour markov with steady-state standard deviation $\sigma_{ss} = 10 \ \mu$g. For each accelerometer's axis, the markov bias b_a evolves as

$$\dot{b}_a = -\frac{1}{\tau}b_a + \nu, \tag{1}$$

where $\tau = 3600$s and ν is a zero-mean white process with spectral density $S_\nu = \sigma_{ss}^2/(2\tau)$. In order to establish to which accuracy this markov bias can be estimated, we assume a continuous Kalman filter, we also assume no non-gravitational forces acting on the vehicle, therefore the accelerometer measurement is

$$y = b_a + \eta \tag{2}$$

---

[*]`http://www.esa.int/esaMI/Space_In_Bytes/SEM7FXJ26DF_0.html`

for each axis. The velocity random walk η is a zero-mean white process, a spectral density $S_\eta = (10 \ \mu g \sqrt{s})^2$ is assumed, which is a relatively good value. The estimate of the markov bias evolves as

$$\dot{\hat{b}}_a = -\frac{1}{\tau}\hat{b}_a + K(y - \hat{b}_a), \tag{3}$$

where $K = P/S_\eta$ and P is the estimation error variance evolving as

$$\dot{P} = -\frac{2}{\tau}P + \frac{2}{\tau}\sigma_{ss}^2 - P^2/S_\eta. \tag{4}$$

After some algebra it follows that the steady-state value of the estimation error standard deviation is $\sqrt{P_{ss}} = 1.5\mu g$. Even under the optimistic assumptions of this example the estimation error of the markov bias is 15 times bigger than drag. When using the compensated accelerometer measurement to propagate the state an additional error source is the VRW. During non-thrusting phases it is therefore much more accurate not to use the accelerometer to propagate the state but to use a simple drag model.

DUAL ACCELEROMETER USAGE STRATEGY

In all spacecraft missions the authors are aware of accelerometers are thresholded during orbital coast flight (sometimes this operation is referred to as accelerometer gating). In the majority of these missions the accelerometer bias is estimated to improve the navigation solution. The estimation occurs in either of two ways. A common solution is to include the accelerometer bias as a state in the filter and to estimate it through external measurements and the correlations built during maneuvers. The issue with this approach is that when maneuvers occur far apart the estimate degrades in-between maneuvers, often resulting in a poor knowledge of the bias when the subsequent maneuver occurs. The usual solution to this problem is to have an external estimator of the accelerometer bias. While this second solution usually produces good results, it completely ignores the inevitable correlation between the states in the filter and the accelerometer bias estimate. To optimally account for this correlation we propose an integrated filter that uses the estimate of the bias during maneuvers and estimates it during coast flight.

Accelerometer measurements fed to the navigation filter are usually integrated accelerations over the last time step and they are compensated for sculling errors. Sculling compensation means that the effects of the rotation of the vehicle during the time step are compensated and the measurement $\Delta\tilde{\mathbf{v}}_k^b$ is an inertial change in velocity between times t_{k-1} and t_k coordinatized in the body-fixed frame at time t_k. When the filter is called it first propagates the position ($\mathbf{r}$), velocity ($\mathbf{v}$), and accelerometer bias ($\mathbf{b}$) to the current IMU time t_k as

$$\frac{d}{dt}\hat{\mathbf{r}}^i = \hat{\mathbf{v}}^i \tag{5}$$

$$\frac{d}{dt}\hat{\mathbf{v}}^i = \hat{\mathbf{g}}^i + \hat{\mathbf{a}}^i \tag{6}$$

$$\frac{d}{dt}\hat{\mathbf{b}}^b = -\frac{1}{\tau}\mathbf{b}_a^b. \tag{7}$$

When the accelerometer measurement is above a threshold the estimated non-gravitational acceleration $\hat{\mathbf{a}}^i$ is obtained from the accelerometer measurement $\hat{\mathbf{a}}^i = \mathbf{T}_b^i(t_k) \left(\Delta\tilde{\mathbf{v}}_k^b/\Delta t - \hat{\mathbf{b}}^b\right)$. When the measurement is below the threshold $\hat{\mathbf{a}}^i$ is either zero or a model of drag, depending on the application. Matrix $\mathbf{T}_b^i(t_k)$ is the coordinate transformation from the body-fixed frame at time t_k to the inertial frame. Other states such as attitude can easily be incorporated in the filter.

When the accelerometer is included during propagation the state is only updated with external measurements. When the accelerometer is thresholded an estimate of the measurement $\Delta\hat{\mathbf{v}}_k^b$ is formed. This estimate is given by

$$\Delta\hat{\mathbf{v}}_k^b = \int_{t_{k-1}}^{t_k} (\mathbf{b}_a^b + \mathbf{d}^b)dt = \tau\left(e^{\Delta t/\tau} - 1\right)\mathbf{b}(t_k) + \int_{t_{k-1}}^{t_k} \mathbf{d}^b dt \simeq \Delta t\left(\mathbf{b}(t_k) + \mathbf{d}^b\right), \quad (8)$$

The measurement mapping matrix for the accelerometer measurement, $\mathbf{H}_a$ is a $3 \times n$ matrix, where n is the number of states in the filter. Matrix $\mathbf{H}_a$ has zeros everywhere except for an identity matrix times Δt at the 3×3 block corresponding the accelerometer bias state. The Kalman gain is calculated as usual

$$\mathbf{K}_k = \mathbf{P}_k^- \mathbf{H}_a^{\mathrm{T}}(\mathbf{H}_a\mathbf{P}_k^-\mathbf{H}^{\mathrm{T}} + \mathbf{R}_a)^{-1}, \quad (9)$$

where $\mathbf{P}_k^-$ is the *a priori* estimation error covariance matrix and $\mathbf{R}_a$ is the accelerometer noise covariance. The accelerometer white noise is expressed in terms of a velocity random walk with an associated spectral density $\mathbf{S}_a$ whose units are the square of $m/s/\sqrt{s}$ or, more frequently, $\mu g\sqrt{s}$. Therefore the covariance of the noise over an IMU step Δt is given by

$$\mathbf{R}_a = \mathbf{S}_a \Delta t. \quad (10)$$

It is not desirable to update all the states, only the accelerometer bias should be updated. Therefore a consider gain $\mathbf{K}_k^*$ is formed by zeroing all the rows of $\mathbf{K}_k$ corresponding to the other states. Since the new gain is not optimal the Joseph's formula is used to obtain the *a posteriori* covariance

$$\mathbf{P}_k^+ = (\mathbf{I}_{n\times n} - \mathbf{K}_k^*\mathbf{H}_a) \, \mathbf{P}_k^- \, (\mathbf{I}_{n\times n} - \mathbf{K}_k^*\mathbf{H}_a)^{\mathrm{T}} + \mathbf{K}_k^*\mathbf{R}_a(\mathbf{K}_k^*)^{\mathrm{T}}. \quad (11)$$

The state is updated as

$$\hat{\mathbf{x}}_k^+ = \hat{\mathbf{x}}_k^- + \mathbf{K}_k^* \left(\Delta\tilde{\mathbf{v}}_k^b - \Delta\hat{\mathbf{v}}_k^b\right). \quad (12)$$

The choice of the threshold value is usually driven by the thruster size, the accelerometer accuracy, and engineering judgement. A good rule of thumbs is to threshold the accelerometer when the measurement is below the 3σ value of the sum of the bias and noise, assumed independent

$$(\Delta\tilde{\mathbf{v}}_k^b)^{\mathrm{T}}\Delta\tilde{\mathbf{v}}_k^b < 9 \left(\mathrm{trace}\,\mathbf{B}_a\Delta t^2 + \mathrm{trace}\,\mathbf{S}_a\Delta t\right), \quad (13)$$

where $\mathbf{B}_a$ is the accelerometer bias covariance from the IMU specifications. If $\Delta\tilde{\mathbf{v}}_k^b$ is compensated with the estimate of the bias, $\mathbf{B}_a$ is replaced with the accuracy of the bias estimate. It is also possible to choose a non-constant threshold

$$(\Delta\tilde{\mathbf{v}}_k^b - \hat{\mathbf{b}}^b\Delta t)^{\mathrm{T}}(\Delta\tilde{\mathbf{v}}_k^b - \hat{\mathbf{b}}^b\Delta t) < 9 \left(\mathrm{trace}\,\mathbf{P}_{aa}^-\Delta t^2 + \mathrm{trace}\,\mathbf{S}_a\Delta t\right), \quad (14)$$

where $\mathbf{P}_{aa}^{-}$ is the 3×3 portion of the covariance corresponding to the accelerometer bias state. Spacecrafts usually operate at low angular rates, but in case of high rates the term $\hat{\mathbf{b}}^{b}\Delta t$ in Eq. (14) needs to be replaced by

$$\int_{t_{k-1}}^{t_k} \mathbf{T}_{b(\tau)}^{b(t_k)} \mathbf{b}^{b}(\tau)\, d\tau, \tag{15}$$

where $\mathbf{T}_{b(\tau)}^{b(t_k)}$ is the transformation matrix that takes the vehicle's body frame at time τ into the body frame at time t_k.

This section assumes that the entire accelerometer measurement is either applied or thresholded, it is also possible to develop similar algorithms by considering the measurement from each axis independently.

NUMERICAL RESULTS

An orbital rendezvous is used as an example. The target spacecraft is placed on a circular 400km orbit. The chaser vehicle is placed in a circular orbit 4km below the target and 14km behind. At a downrange of 13.2km an altitude raise maneuver is commanded. This maneuver is a 135 degree lambert targeting taking the chaser to 1.4km below and 4.3km behind the target. A clean up maneuver is performed half the way during this transfer. A circularization maneuver is performed once the end of the transfer (2030s). A third maneuver is performed that will take the chaser 500m below the target with zero relative velocity. Figure 1 shows the relative trajectory. The origin is the location of the target, while the line represent the relative position in time. The y-axis is the altitude counted positive below the target, while the x-axis is downrange.
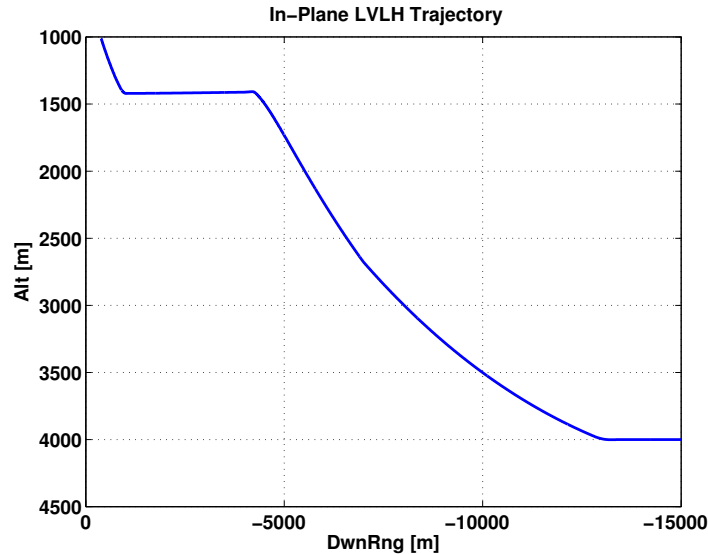

Figure 1. Relative In-Plane LVLH Trajectory

5

The simulated true environment contains a 9 by 9 gravity model and atmospheric drag. The filter is a nine state filter with relative position, velocity, and accelerometer bias. The filter's propagation includes J2 effects and no drag. The chaser vehicle has a 20N thruster and a mass of 1000kg. The accelerometer errors are given in Table 1.

Error Type	1σ Error	Units
Time Constant	3600	s
Markov Bias	100	μg
Velocity Random Walk	100	μg$\sqrt{\text{s}}$

Table 1. Accelerometer Model Error Parameters

Together with the accelerometer there is a long range radar whose errors are shown in Table 2. The radar provides range to the target as well as azimuth and elevation to it.

Error Type	1σ Error	Units
Range Error	5	m
Angles Errors	0.5	deg

Table 2. Radar Model Error Parameters

The initial filter covariance is diagonal with entries as shown in Table 3, while the velocity process noise covariance is $10^{-6}\text{m}^2/\text{s}^3$.

Error Type	1σ Error	Units
Relative Position	10	m
Relative Velocity	0.1	m/s
Accelerometer Bias	100	μg

Table 3. Initial Estimation Errors

Figs. 2 and 3 show the filter's performance without thresholding the accelerometer (i.e. the accelerometer measurement is always used to propagate the vehicle state). The lines show the estimation error standard deviation. It can be seen that the estimate becomes progressively better as the chaser approaches the target. At the very beginning of the simulation the estimate of velocity degrades, this fact is due to the accelerometers errors.

Figs. 4 and 5 show the filter's performance with accelerometer thresholding. The overall performance of the system improves, and especially during coast phases the unceatinty of the state is greatly reduced with respect to the previous case. The times at which the maneuvers occur are easily visible from the velocity error plot. During the maneuver a spike in velocity error occurs, which drives an increase of position error as well.
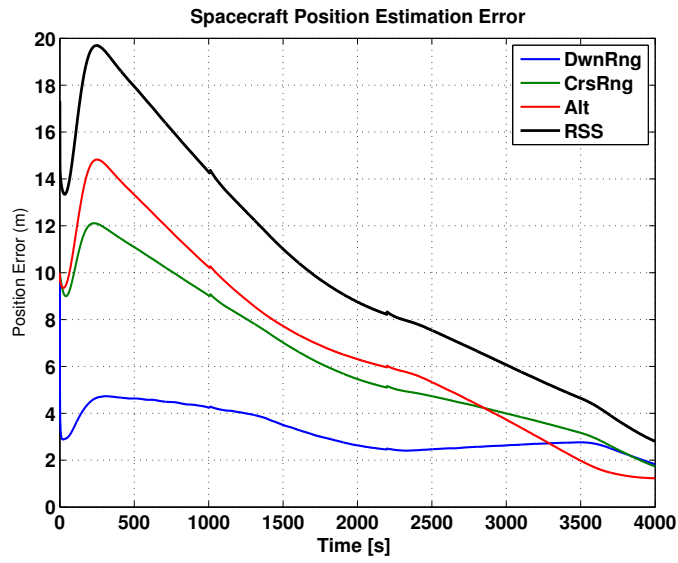
6

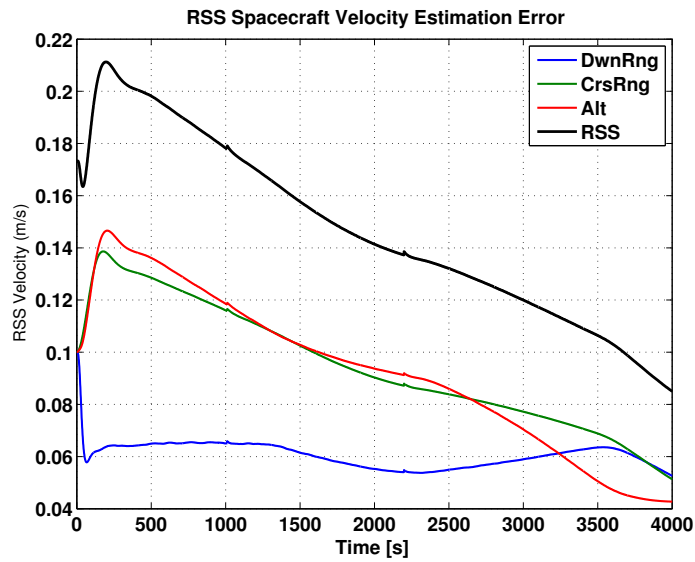**Figure 2. Position Estimation Error Without Thresholding**

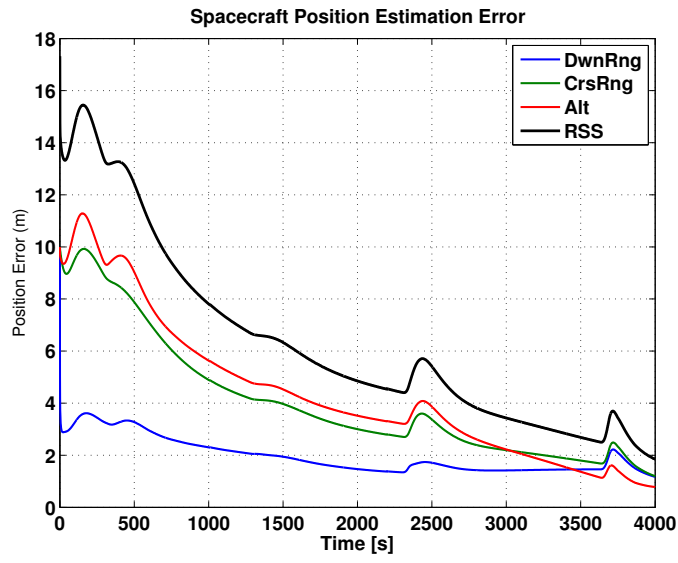**Figure 3. Velocity Estimation Error Without Thresholding**

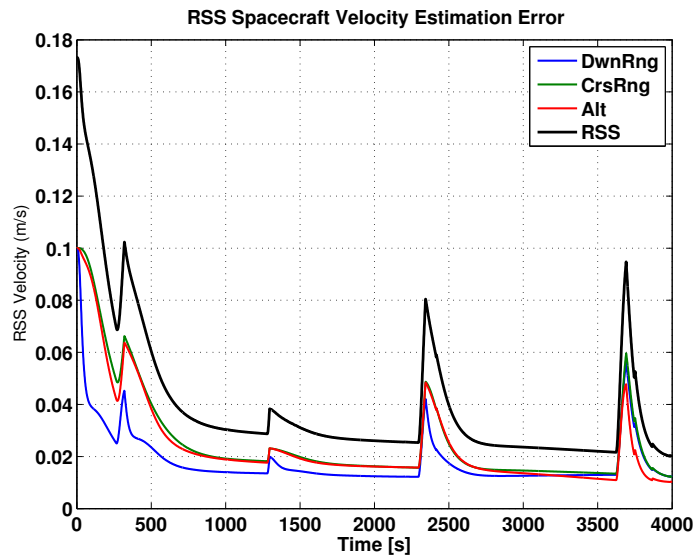**Figure 4. Position Estimation Error With Thresholding**

Figure 5. Velocity Estimation Error With Thresholding

8

Figs. 6 and 7 show the filter's performance when the accelerometer bias is estimated from the accelerometer measurements outside maneuvers. Figs. 8 and 9 show a direct comparison of the three methods. The proposed algorithm performs the best and it can be seen that the new algorithm outperforms the simple thresholding scheme while firing of the thrusters. Fig. 10 gives great insight on the reason of the various filters performances. The green line is the scheme in which the accelerometer measurement is always incorporated to propagate the state. After a first period in which the uncertainty decreases relatively fast, the filter estimates the bias to its full capability and further improvements are slow and due to the progressive reduced distance between the two vehicles. The filter estimates the accelerometer bias through radar measurements taking advantage of the correlations built during the propagation phase. The red line shows the proposed algorithm and it can be seen that the bias uncertainty decreases much faster and to a much lower level. The reason is that the accelerometer bias is estimated directly from the accelerometer measurements and not deduced from radar measurements. The maneuvers are clearly visible as little spikes in the accelerometer bias estimation error. The reason is that the small thrusters cause long burn times and during maneuvers no measurement is available to directly estimate the bias. These two effects result in degradation of the estimate during maneuvers, followed by an improvement once the maneuver ended. While the simple thresholding scheme outperforms the no-thresholding algorithm in estimating position and velocity, it provides the worst estimate of acceleration bias as seen by the black line in Fig. 10. Until the first maneuver no correlation exists therefore the bias is not estimated at all and remains at the Markov steady-state value. After the first maneuver the built correlation allows the filter to estimate the bias through radar measurements until a point is reached in which the quantities have de-correlated enough that the estimates starts degrading again. This pattern is repeated after subsequent maneuvers. The large accelerometer bias estimation errors are the reason of the large velocity error spikes in Fig. 5.

CONCLUSIONS

This papers presents a dual accelerometer usage in an orbital Kalman filter. The accelerometer is both used to propagate position and velocity during maneuvers and to update the accelerometer bias state outside of maneuvers. The advantage of this approach is its superior performance than simply thresholding the accelerometer. The correlation between accelerometer bias and position and velocity during the maneuvers is not sufficient to adequately estimate the bias during coast flight. Therefore the estimate of the bias degrades outside of maneuvers adding considerable uncertainty during subsequent maneuvers. A common solution to this problem is to estimate the accelerometer bias outside of the navigation filter just prior to a maneuver is performed. A simple averaging scheme is often used, but a Kalman filter is also a possibility. The advantage of the proposed scheme over a separate bias estimator is that a single estimator is globally optimal because it accounts for all the correlations.
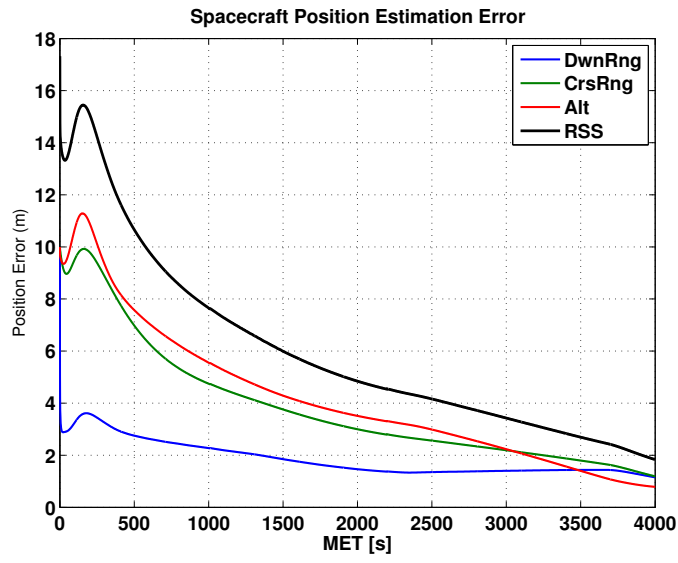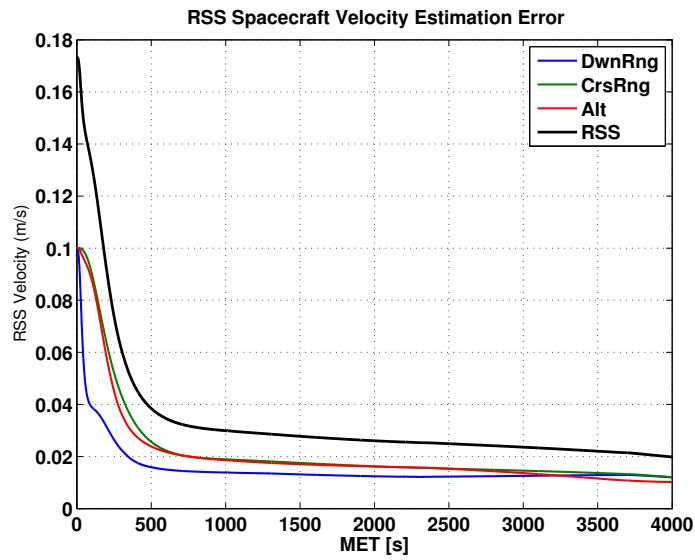
9

Figure 6. Position Estimation Error New Algorithm

Figure 7. Velocity Estimation Error New Algorithm
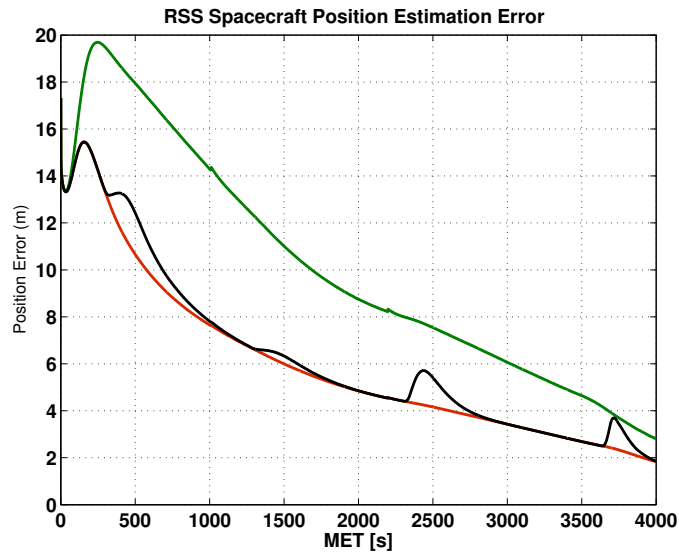
10

RSS Spacecraft Position Estimation Error

Figure 8   Comparison of position estimation error, green line shows no threshold, black line with threshold and red line is the new algorithm
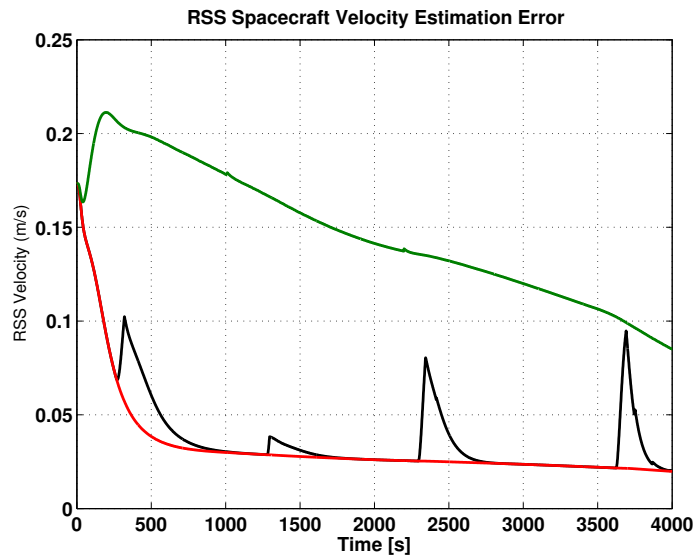
RSS Spacecraft Velocity Estimation Error

Figure 9   Comparison of velocity estimation error, green line shows no threshold, black line with threshold and red line is the new algorithm
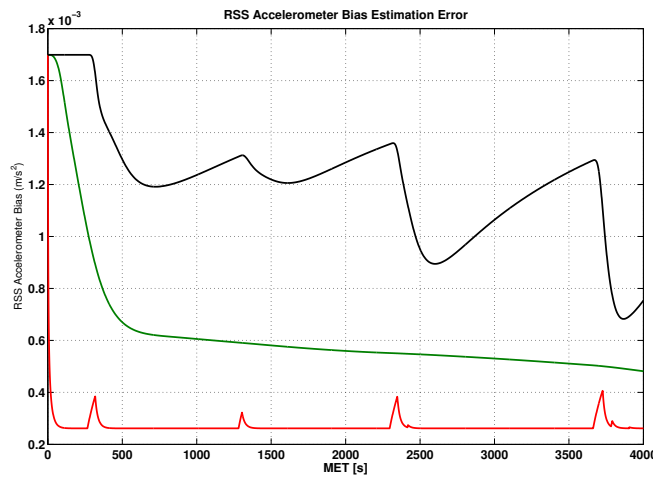
11

Figure 10   Comparison of accelerometer bias estimation error, green line shows no threshold, black line with threshold and red line is the new algorithm

REFERENCES

[1] Kalman, R. E., "A New Approach to Linear Filtering and Prediction Problems," *Journal of Basic Engineering*, Vol. 82, No. Series D, March 1960, pp. 35–45.

[2] Kalman, R. E. and Bucy, R. S., "New Results in Linear Filtering and Prediction," *Journal of Basic Engineering*, Vol. 83, No. Series D, March 1961, pp. 95–108.

[3] Bishop, R. H., Crain, T. P., and Azimov, D. M., "Sensitivity of Mars Entry Navigation Errors to Sensed Accelerometer Threshold," *Proceedings of the AIAA Guidance, Navigation, and Control Conference*, Austin, TX, 11-14 August 2003, AIAA-2003-5749.

[4] Clark, F. D., Spehar, P. T., Brazzel, J. P., and Hinkel, H. D., "Laser-Based Relative Navigation and Guidance for Space Shuttle Proximity Operations," *Proceedings of the 26th Annual AAS Guidance and Control Conference*, Breckenridge, CO, February 5–9 2003, pp. 521–529.

[5] Zanetti, R. and Bishop, R. H., "Adaptive Entry Navigation Using Inertial Measurements," *Proceedings of the 2007 AAS/AIAA Spaceflight Mechanics Meeting held January 28 – February 1, 2007, Sedona, Arizona*, Vol. 127 of *Advances in the Astronautical Sciences*, 2007, pp. 457–470, AAS 07-129.

[6] Brown, R. G. and Hwang, P. Y., *Introduction To Random Signals And Applied Kalman Filtering*, John Wiley and Sons, 3rd ed., 1997.